ACS APPLIED MATERIALS & INTERFACES

Research Article

www.acsami.org

Enhanced Performance of Polymer Solar Cells using PEDOT:PSS Doped with Fe_3O_4 Magnetic Nanoparticles Aligned by an External Magnetostatic Field as an Anode Buffer Layer

Kai Wang,[†,‡] Chao Yi,[†,‡] Xiaowen Hu,[‡] Chang Liu,[‡] Yan Sun,[‡] Jianhui Hou,[§] Yongfang Li,[§] Jie Zheng,[⊥] Steven Chuang,[‡] Alamgir Karim,[‡] and Xiong Gong*[,‡]

[‡]College of Polymer Science and Polymer Engineering and [⊥]Department of Chemical and Biomolecular Engineering, The University of Akron, Akron, Ohio 44325, United States

[§]Institute of Chemistry, Chinese Academy of Science, Beijing 100190, P. R. China

ABSTRACT: Low efficiency and poor stability are two major obstacles limiting the manufacturing of renewable and cost-effective polymer solar cell (PSCs). To address these problems, solution-processed poly(3,4-ethylenedioxythiophene):poly(styrenesulfonate) (PEDOT:PSS) doped with Fe_3O_4 magnetic nanoparticles ((PEDOT:PSS):Fe_3O_4), and above (PEDOT:PSS):Fe_3O_4 thin film aligned by an external magnetostatic field ([(PEDOT:PSS):Fe_3O_4] W/H) were used as the anode buffer layer for PSCs, respectively. As compared with PSCs with PEDOT:PSS as an anode buffer layer, 38.5% enhanced efficiency and twice improved stability are observed from PSCs incorporated with [(PEDOT:PSS):Fe_3O_4] W/H anode buffer layer. It was found that enhanced efficiency and improved stability resulted from a combination of reduced acidity of PEDOT:PSS and enhanced electrical conductivity that originated from generated counterions and the paramagnetism of Fe_3O_4 magnetic nanoparticles by an external magnetostatic field.

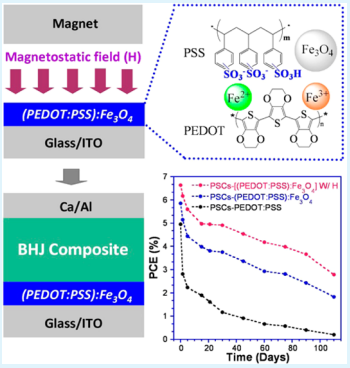

KEYWORDS: *polymer solar cells, efficiency, stability, magnetic nanoparticles, external magnetostatic field*

INTRODUCTION

Bulk heterojunction (BHJ) polymer solar cells (PSCs) have shown great potential as one of the renewable and cost-effective energy sources.[1−3] BHJ PSCs are generally consisting of an active layer of conjugated polymer blended with fullerene derivative sandwiched by an indium tin oxide (ITO) anode and a metal cathode. Typically, poly(3,4-ethylenedioxythiophene):poly(styrenesulfonate) (PEDOT:PSS) is used as an anode buffer layer to smooth the surface of ITO and reduce the contact resistance between BHJ composite active layer and the ITO anode.[4] However, the acidic PEDOT:PSS etches ITO substrate and thus degrades the performance of BHJ PSCs.[5−7] Moreover, the thin film of PEDOT:PSS is unstable and possesses low conductivity (ca. < 1 S cm^{-1}),[8,9] which limits the development of PSCs with high efficiency. In order to circumvent these problems, p-type metal oxides such as MoO_3, NiO, V_2O_5 were used to substitute PEDOT:PSS buffer layer.[8,10−12] The power conversion efficiencies (PCEs) of PSCs incorporating with vacuum-deposited metal oxide as a hole extraction layer were comparable to those using PEDOT:PSS anode buffer layer,[13] whereas the PCEs of PSCs incorporating with solution-processed metal oxides were inferior than those with PEDOT:PSS.[14] Compared with p-type metal oxides, PEDOT:PSS shows advantages in fabrication simplicity and device efficiency but disadvantages on stability due to its acidic nature. Moreover, as anode buffer layer, the electrical conductivity of PEDOT:PSS can be improved because of its constitutional and structural characteristics. Therefore, reducing the acidity and enhancing the electrical conductivity of PEDOT:PSS is probably a promising approach to realize low-cost manufacturing PSCs with high efficiency and good stability.[22−25]

Several methods have been reported for enhancement of the electrical conductivity of PEDOT:PSS, for example, PEDOT:PSS doped with an organic compound, or an ionic liquid, or an anionic surfactant was used for minimizing its acidity.[15] Recently, Xie et al. observed a 50% enhanced PCE from PSCs by using PEDOT:PSS doped with a cationic surfactant as an anode buffer layer.[16] Huang et al. reported high-performance PSCs by using one-dimensional n-PEDOT as an anode buffer layer.[17] However, the improvements in PCEs through these methods were still insufficient and new approaches need to be explored.

Here, we report a facile method to enhance the efficiency and improve the stability of PSCs. By using a thin film fabricated from the solution of PEDOT:PSS doped with Fe_3O_4 magnetic nanoparticles (MNP) (represented by (PEDOT:PSS):Fe_3O_4) as an anode buffer layer, and above (PEDOT:PSS):Fe_3O_4 thin film aligned by an external magnetostatic field (represented by [(PEDOT:PSS):Fe_3O_4] W/H), as an anode buffer, respec-

Received: May 19, 2014
Accepted: July 1, 2014
Published: July 1, 2014

tively, significantly enhanced efficiency and improved stability of PSCs were observed.

EXPERIMENTAL SECTION

Materials. The PBDTTT-C-T was synthesized by Yongfang Li's group and $PC_{71}BM$ was purchased from 1-Material Inc. The PEDOT:PSS (Clevios HTL Solar) was purchased from Heraeus and used as received. The Fe_3O_4 MNP H_2O dispersion solution was bought from Ocean Nano Tech LLC and used as received. All the film of (PEDOT:PSS):Fe_3O_4) and [(PEDOT:PSS):Fe_3O_4] W/H were casted from the solution of PEDOT:PSS doped with Fe_3O_4 MNP To fabricate the film of [(PEDOT:PSS):Fe_3O_4] W/H, a magnetostatic field with a magnetic induction intensity of 500 G was applied in vertical direction during annealing process. The thickness of PEDOT:PSS, (PEDOT:PSS):Fe_3O_4) and [(PEDOT:PSS):Fe_3O_4] W/H are ~40 nm.

Film Characterization. Tapping-mode atomic force microscopy (AFM) images were obtained by using a NanoScope NS3A system (Digital Instrument) to observe the surface morphologies and thicknesses of various thin films. Bright-field TEM experiments were carried out with a JEOL transmission electron microscope using an accelerating voltage of 120 kV. XPS images were measured by a PHI 5000 Versa Probe II scanning XPS microprobe to identify the components on the surface of all the films.

Electrical Conductivity of Thin Films. Four point probe method was utilized to measure the electrical conductivity of the thin films. The thin films of PEDOT:PSS, (PEDOT:PSS):Fe_3O_4, and [(PEDOT:PSS):Fe_3O_4] W/H were deposited on precleaned glass substrates with an area of 1 × 1 cm^2. The thicknesses of above three different thin films are ~40 nm. Aluminum contact was thermally deposited on the four corners of the films. The electrical conductivities of thin film were calculated as $\sigma = 1/(R_S t)$, where R_S is the sheet resistance of the films measured by the four-point probe method, and t is the thickness of the films.

PSC Fabrication. The device structure of PSCs is ITO/anode buffer layer/polymer:fullerene BHJ composite/Ca/Al, where the anode buffer layer with a thickness of 40 nm (± 5 nm) is PEDOT:PSS, (PEDOT:PSS):Fe_3O_4, and [(PEDOT:PSS):Fe_3O_4] W/H, respectively. First, ITO coated glass slides were cleaned by detergent, followed by ultrasonic washing in deionized water, acetone and isopropanol, and subsequently dried in an oven overnight. After that, the anode buffer layer, PEDOT:PSS or PEDOT:PSS doped with Fe_3O_4 MNP (5% by volume), was spin-coated from the corresponding solutions, respectively. The anode buffer layer, PEDOT:PSS and (PEDOT:PSS):Fe_3O_4 layer coated ITO substrates were annealed at 150 °C for 10 min in air. For the anode buffer layer [(PEDOT:PSS):Fe_3O_4] W/H, a magnet is directly put on the top of the thin film during the thermal annealing process. After that, all the anode buffer layer coated ITO substrates were transferred into the glovebox with N_2 atmosphere. BHJ composite of PBDTTT-C-T:$PC_{71}BM$ (1:1.5, weight ratio) was spin-coated onto the top of buffer layer from ortho-dichlorobenzene (o-DCB) solution. The thickness of BHJ active layer was ~140 nm. Finally, metal top electrode, Ca and Al were sequentially deposited onto BHJ active layer in vacuum onto with a pressure of ca. 4 × 10^{-6} mbar. The active area of PSCs was measured to be 0.045 cm^2.

PSC Characterization. The current-density versus voltage (J–V) curves characteristics were measured using a Keithley 2400 Source Measure Unit. The solar cells were characterized using a Newport Air Mass 1.5 Global (Am 1.5G) full spectrum solar simulator with an intensity of 100 mW cm^{-2}. The light intensity was determined by a monosilicon detector (with KG-5 visible color filter) calibrated by National Renewable Energy Laboratory (NREL) to reduce spectral mismatch. The incident photon-to-electron conversion efficiency (IPCE) spectra of PSCs were measured by solar cell quantum efficiency measurement system (QEX10) from PV Measurements. The impedance spectra (IS) were obtained using a HP 4194A impedance/gain-phase analyzer, all under illumination, with an oscillating voltage of 10 mV and frequency of 1 Hz to 1 MHz. PSCs were held at their respective open circuit potentials obtained from the J–V measurements, while the IS spectrum was recorded.

RESULTS AND DISCUSSION

Sample Preparation and Characterization. Fe_3O_4 MNP was selected to modify the electrical properties of PEDOT:PSS because of its special electrical, chemical, magnetic, optical, and anticorrosive properties.[18] Moreover, it is expected that the reaction between basic Fe_3O_4 MNP and acidic PEDOT:PSS would reduce the acidity of PEDOT:PSS and simultaneously generate Fe^{3+} ions, thus resulting in high electrical conductivity and enhanced stability.

In order to verify whether the Fe_3O_4 MNP was doped into PEDOT:PSS or not, pH value of the mixed solution of PEDOT:PSS and Fe_3O_4 MNP was checked and compared with that of pristine PEDOT:PSS. The pH value of the solution of PEDOT:PSS became 5–6 from 1–2[19,20] after doping 5% Fe_3O_4 MNP into the solution of PEDOT:PSS. The change of pH value indicated that the sulfonic acid in PSS was reacted with Fe_3O_4 MNP and generated the counterions, Fe^{3+}, at the same time. In order to confirm that Fe^{3+} was generated by above reaction, the solution was further checked by a coordination reaction between the Fe^{3+} ions and the thiocyanate ions (SCN^-). It was found that the color of potassium thiocyanate solution quickly changed from colorless to red upon addition of a few drops of the solution of (PEDOT:PSS):Fe_3O_4. The red color originated from the iron thiocyanate complex ($[Fe(SCN)_n]^{3-n}$ (n = 1–6)),[21] which was formed by the Fe^{3+} ions coordinated with SCN^-. These results demonstrate that Fe_3O_4 MNP reacted with PEDOT:PSS. As a result, extra Fe^{3+} ions were generated and the acidity of PEDOT:PSS was reduced. Therefore, with the introduction of extra Fe^{3+} ions, the morphology of PEDOT:PSS film is expected to be changed.[22]

Figure 1 presents the transmittance spectra of pristine PEDOT:PSS, pristine Fe_3O_4 MNP, and (PEDOT:PSS):Fe_3O_4 thin films. The spectrum of pristine Fe_3O_4 MNP thin film shows 97% transmittance from 400 to 1100 nm. The transmittance of (PEDOT:PSS):Fe_3O_4 thin film is greater than that of pristine PEDOT:PSS. The transmittance spectrum of (PEDOT:PSS):Fe_3O_4 thin film is a superposition of pristine

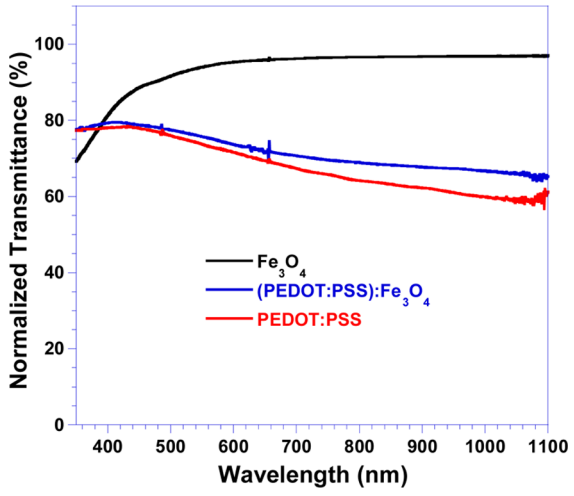

Figure 1. Transmittance spectra of thin films of PEDOT:PSS, Fe_3O_4 magnetic nanoparticles, and (PEDOT:PSS): Fe_3O_4 magnetic nanoparticles.

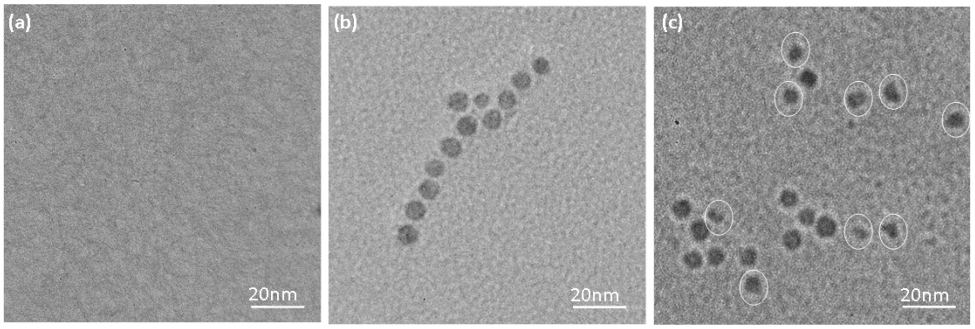

Figure 2. TEM bright-field images of (a) pristine PEDOT:PSS, (b) pristine Fe_3O_4 magnetic nanoparticles, and (c) (PEDOT:PSS):Fe_3O_4 magnetic nanoparticles.

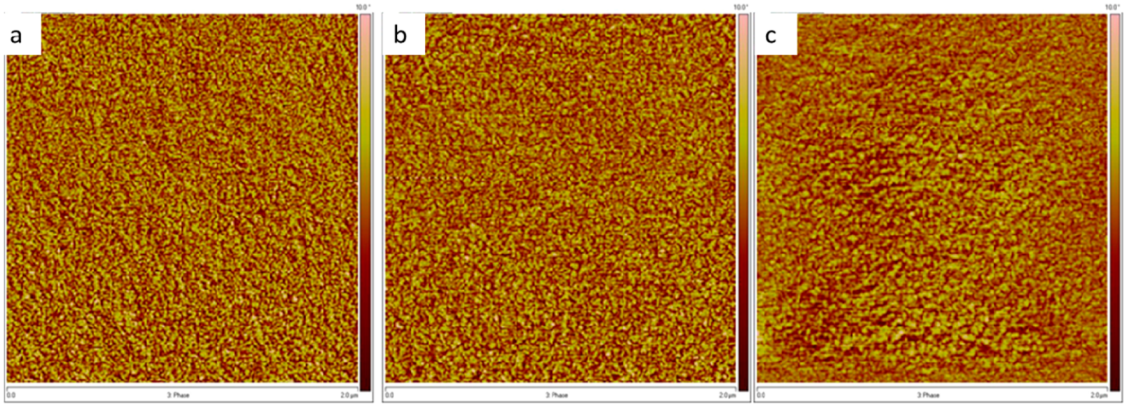

Figure 3. AFM phase images on 2 μm × 2 μm: (a) PEDOT:PSS; (b) (PEDOT:PSS):Fe_3O_4; and (c) [(PEDOT:PSS):Fe_3O_4)] W/H.

PEDOT:PSS and Fe_3O_4 MNP. Good transmittance from 400 to 1100 nm indicates more visible light is able to pass through the (PEDOT:PSS):Fe_3O_4 thin film into the BHJ active layer.

As expected, the morphology of PEDOT:PSS film would change with introduction of extra Fe_3O_4 MNP into PEDOT:PSS.[22] The thin film morphologies were investigated by transmission electron microscopy (TEM). A comparison of bright field TEM images of pristine PEDOT:PSS, pristine Fe_3O_4 MNP and (PEDOT:PSS):Fe_3O_4 thin films is shown in Figure 2. The thin film of pristine PEDOT:PSS is uniform and homogeneous. The thin films of pristine Fe_3O_4 MNP and (PEDOT:PSS):Fe_3O_4 are uniform as well. However, the Fe_3O_4 MNP is clearly observed from the latter two samples. Interestingly, the mean sizes of Fe_3O_4 MNP presents in PEDOT:PSS thin film were evidently smaller than those of pristine Fe_3O_4 MNP and the shape of Fe_3O_4 MNP became irregular. The spherical particles look like to have been "bitten" by PEDOT:PSS, as shown in Figure 2c. This is attributed to partially etched Fe_3O_4 MNP by sulfonic acid groups. All these results provide further evidence suggesting that Fe_3O_4 MNP was reacted with PEDOT:PSS, generating extra counter Fe^{3+} ions and reducing acidity of PEDOT:PSS. Thus, we expect high electrical conductivity from thin film of (PEDOT:PSS):Fe_3O_4.

Because of the generation of Fe^{3+} ions, the space between PEDOT and PSS chains could be changed by the screen effect.[22,23] To confirm this hypothesis, the thin film morphologies of PEDOT:PSS, (PEDOT:PSS):Fe_3O_4 and the [(PEDOT:PSS):Fe_3O_4] W/H were further investigated by AFM. AFM images of PEDOT:PSS, (PEDOT:PSS):Fe_3O_4 and [(PEDOT:PSS):Fe_3O_4] W/H are shown in Figure 3. As compared with pristine PEDOT:PSS (Figure 3a), aggregated PEDOT and voids in the images of (PEDOT:PSS):Fe_3O_4 (Figure 3b) and [(PEDOT:PSS):Fe_3O_4] W/H (Figure 3c) suggested that the film morphology of PEDOT:PSS was changed after the doping of PEDOT:PSS with Fe_3O_4 MNP. Moreover, because of the screen effect from the generated Fe^{3+} ions, larger PEDOT domains were formed, which would facilitate hole transport through the thin film.[22,23] As shown in Figure 3, the domain size of PEDOT is enlarged after doping with Fe_3O_4 MNP. After above thin film aligned by an external magnetic field, the PEDOT domain becomes even larger. All these imply that enhanced electrical conductivities are expected from PEDOT:PSS):Fe_3O_4 and [(PEDOT:PSS):Fe_3O_4] W/H thin films.

Figure 4 shows the current density−voltage (J−V) characterization of the diodes with a structure of ITO/anode buffer layer/Al, where anode buffer layers are PEDOT:PSS, (PEDOT:PSS):Fe_3O_4 and [(PEDOT:PSS):Fe_3O_4] W/H, respectively. The different slopes of J−V curves indicate that these thin films possess different electrical conductivities. Greater slop indicates better conductivity. Thus, at the same biased voltage, the electrical conductivity of [(PEDOT:PSS):-Fe_3O_4] W/H is the largest, followed by (PEDOT:PSS):Fe_3O_4, whereas PEDOT:PSS is the least conductive. To further confirm it, we utilized the four-point probe method to measure the electrical conductivity of the thin films. The electrical conductivity of PEDOT:PSS thin film is 2.00 ± 0.09 S/cm, which is a little bit lower than the value from the manufacturer.[8,9,24] However, the electrical conductivities of (PEDOT:PSS):Fe_3O_4 and [(PEDOT:PSS):Fe_3O_4] W/H thin films are 3.00 ± 0.08 S/cm and 4.16 ± 0.08 S/cm, respectively. The electrical conductivity of (PEDOT:PSS):Fe_3O_4 is higher than that of PEDOT:PSS, which is consistent with H. S. Liu et al.'s report.[25] The latter is 2 times higher than that of

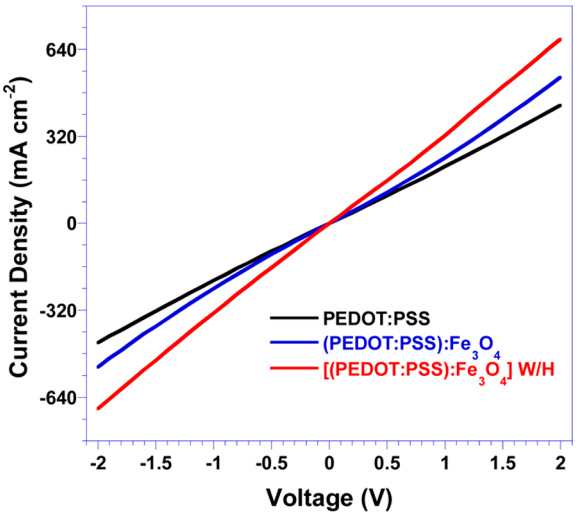

Figure 4. Current−voltage characteristic of a diode with a structure of ITO/anode buffer layer/Al, where anode buffer layer is PEDOT:PSS, or (PEDOT:PSS):Fe_3O_4 or [(PEDOT:PSS):Fe_3O_4)] W/H.

PEDOT:PSS. These results indicate that the electrical conductivityof the [(PEDOT:PSS):Fe_3O_4] W/H thin film is higher than that of (PEDOT:PSS):Fe_3O_4 thin film, which is higher than that of the PEDOT:PSS thin film.

To further confirm such conductivity difference, we measured the surface electrical conductivity of PEDOT:PSS, (PEDOT:PSS):Fe_3O_4 and [(PEDOT:PSS):Fe_3O_4)] W/H by peak force tunneling AFM (PFTUNA).[26] The peak current images of these thin films are presented in Figure 5. The peak current for each measurement is set to 2.0 pA. It is found that the number of highly conductive domains for PEDOT:PSS (Figure 5a) is the smallest, whereas for (PEDOT:PSS):Fe_3O_4 (Figure 5b) is moderate. Thus, surface conductivity of (PEDOT:PSS):Fe_3O_4 is larger than that of PEDOT:PSS. Remarkably, a significant enhancement in surface conductivity was observed from [(PEDOT:PSS):Fe_3O_4)] W/H thin film. Highly conductive domains, which are largest in size among these three samples and well-distributed throughout the whole thin film, were observed from [(PEDOT:PSS):Fe_3O_4)] W/H as shown in Figure 5c. Therefore, the surface electrical conductivity of [(PEDOT:PSS):Fe_3O_4)] W/H is larger than that of (PEDOT:PSS):Fe_3O_4 which is larger than that of PEDOT:PSS. These results are in good agreement with the observation from Figure 4 and four-point probe measurement. This high surface electrical conductivity would facilitate charge transport through the thin film toward the ITO anode, resulting in large J_{SC} in PSCs.[2] Consequently, enhanced device performance is expected from PSCs with [(PEDOT:PSS):-Fe_3O_4)] W/H as an anode buffer layer.[22,23]

Solar Cell Performance. Figure 6 shows a schematic illustration of fabrication procedure of anode buffer layers,

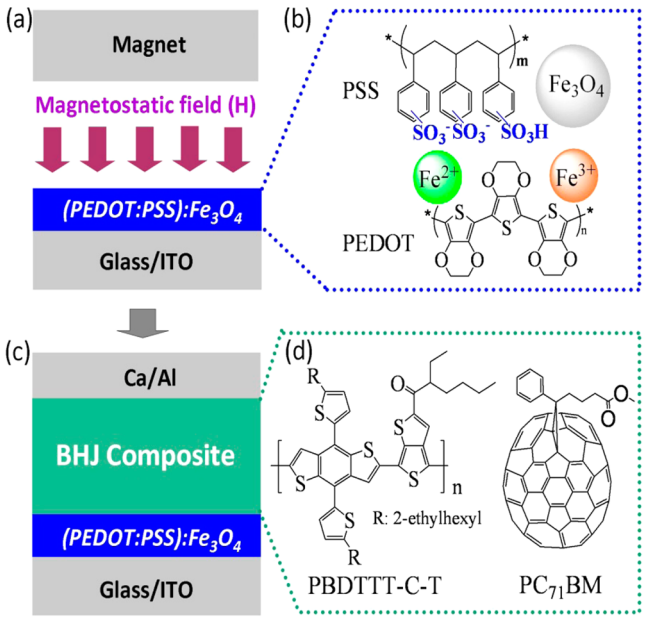

Figure 6. Schematic illustration of (a) fabrication procedure for anode buffer and (b) PEDOT:PSS:Fe_3O_4 buffer layer, (c) conventional device structure of PSCs, and (d) molecular structures of PBDTTT-C-T and $PC_{71}BM$.

(PEDOT:PSS):Fe_3O_4 and [(PEDOT:PSS):Fe_3O_4] W/H, device structure of PSCs, and molecular structures of the electron donor, PBDTTT-C-T (a low bandgap polymer derived from the thienothiophene (TT) and benzo[1,2-b:4,5-b́]dithiophene (BDT) alternating units),[27] and the electron acceptor, $PC_{71}BM$ ([6,6]-phenyl-C_{71}-butyric acid methyl ester). The thin film of (PEDOT:PSS):Fe_3O_4 was casted from the solution of (PEDOT:PSS):Fe_3O_4 (Fe_3O_4: 5% by volume) followed with thermal annealing at 150 °C for 10 min. The thin film of [(PEDOT:PSS):Fe_3O_4] W/H was casted from the solution of (PEDOT:PSS):Fe_3O_4 (Fe_3O_4: 5% by volume) followed with an external magnetostatic field alignment during the thermal annealing treatment. After that, BHJ composite of

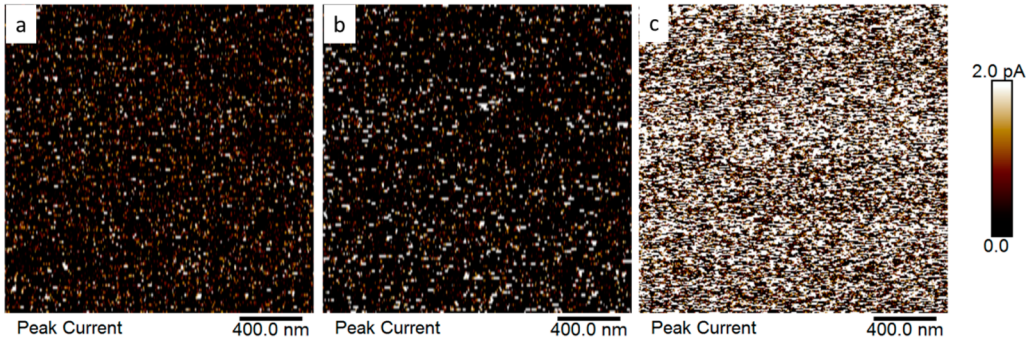

Figure 5. Peak force tunneling AFM phase images on 2 μm × 2 μm: (a) PEDOT:PSS, (b) PEDOT:PSS: Fe_3O_4, and (c) [(PEDOT:PSS):Fe_3O_4)] W/H.

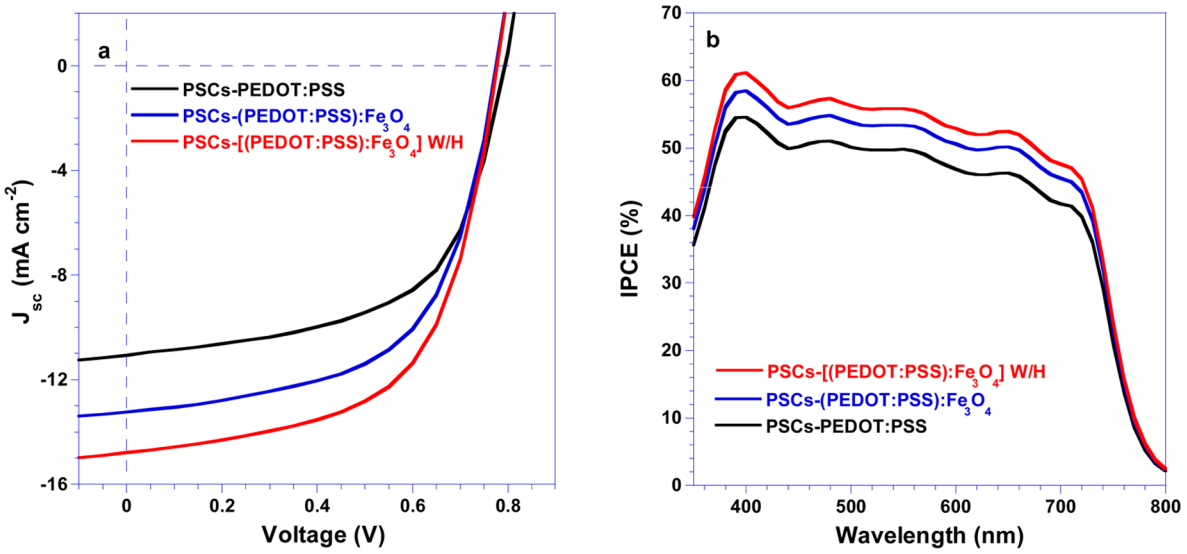

Figure 7. (a) $J-V$ characteristics of PSCs measured under 100 mW cm^{-2} AM 1.5 G illumination, and (b) IPCE spectra of PSCs versus wavelength.

Table 1. Device Performance of PSCs with Three Types of Hole Extracting Layers

polymer solar cells	V_{OC} (V)	J_{SC} (mA cm^{-2})	FF (%)	R_S (Ω cm^2)	R_{SH} (Ω cm^2)	PCE (%)
PSCs-PEDOT:PSS	0.79	10.79	58.0	13.5	625	4.94
(PEDOT:PSS):Fe_3O_4	0.78	12.99	58.0	7.8	649	5.85
[(PEDOT:PSS):Fe_3O_4] W/H	0.78	14.78	59.3	5.9	426	6.84

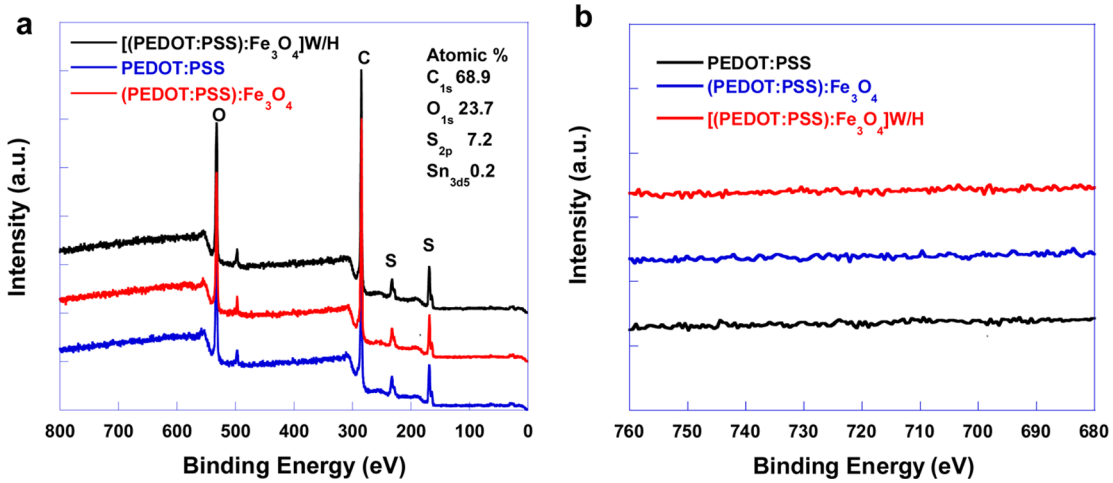

Figure 8. (a) XPS spectra of thin films of PEDOT:PSS, (PEDOT:PSS):Fe_3O_4 and [(PEDOT:PSS):Fe_3O_4] W/H, and (b) partial enlarged spectra.

PBDTTT-C-T:$PC_{71}BM$ (1:1.5 by weight) was spin-coated on the top of either (PEDOT:PSS):Fe_3O_4 or [(PEDOT:PSS):-Fe_3O_4] W/H thin films. Finally, the top electrode (Ca coated with Al) was sequentially thermally deposited onto BHJ layer in vacuum. PSCs with pristine PEDOT:PSS anode buffer was also fabricated as a control device.

The J-V characteristics of PSCs with PEDOT:PSS as an anode buffer layer (represented by PSCs-PEDOT:PSS), PSCs with (PEDOT:PSS):Fe_3O_4 as an anode buffer layer (represented by PSCs-(PEDOT:PSS):Fe_3O_4) and PSCs with [(PEDOT:PSS):Fe_3O_4] W/H as an anode buffer layer (represented by PSCs-[(PEDOT:PSS):Fe_3O_4] W/H), measured under a simulated sun light with air mass 1.5 global (AM 1.5 G) at the light intensity of 100 mW cm^{-2}, are shown in Figure 7a. PSCs-PEDOT:PSS exhibits an V_{OC} of 0.79 V, a short-circuit current density (J_{SC}) of 10.79 mA cm^{-2} and fill factor (FF) of 58.0%, yielding a corresponding PCE of 4.94%. Where PSCs-(PEDOT:PSS):Fe_3O_4 exhibits V_{OC} of 0.78 V, J_{SC} of 12.99 mA cm^{-2}, and FF of 58.0%, yielding a corresponding PCE of 5.85%. This value is about 18% larger than that from PSCs-PEDOT:PSS. PSCs-[(PEDOT:PSS):Fe_3O_4] W/H exhibits V_{OC} of 0.78 V, J_{SC} of 14.78 mA cm^{-2}, and FF of 59.3%, yielding a corresponding PCE of 6.84% which is about 38% higher than those from PSCs-PEDOT:PSS. More than 100 devices were fabricated and less than 5% deviations in PCEs were observed.

We also investigate the PEDOT:PSS doped with different concentrations of Fe_3O_4 MNP. We found that for the large volume percentage of Fe_3O_4 MNP, there would exist insoluble sedimentation in the PEDOT:PSS solution. For the small volume percentage of Fe_3O_4 MNP, the enhancement in PCEs is less than those with 5% Fe_3O_4 MNP.

We also estimated the series resistance (R_S) and shunt resistance (R_{SH}) from the slope of $J-V$ curves at 0 mA cm^{-2} and 0 V, respectively. The R_S and R_{SH} values from these three PSCs are summarized in Table 1. A low R_S from [(PEDOT:PSS):Fe_3O_4] W/H is due to the small contact resistance and bulk resistance of the photoactive material, indicating that high currents will flow through the cell at low applied voltages. The large R_{SH} indicates that shorts or leakages of the photocurrent are minimal in the device.

The PSCs were further characterized by the incident photon to charge carrier efficiency (IPCE) spectroscopy. The IPCE spectra of PSCs are shown in Figure 7b. Apparently, the IPCE values, ranged from 400 to 800 nm for PSCs-[(PEDOT:PSS):-Fe_3O_4] W/H are higher than those of PSCs-(PEDOT:PSS):-Fe_3O_4 and PSCs-PEDOT:PSS. The calculated J_{SC} based on IPCE spectra are 10.36, 12.47, and 14.10 mA cm^{-2} for PSCs-PEDOT:PSS, PSCs-(PEDOT:PSS):Fe_3O_4, and PSCs-[(PEDOT:PSS):Fe_3O_4] W/H, respectively. All these calculated J_{SC} are consistent with the J_{SC} values obtained from $J-V$ characteristics of PSCs.

It is found that all PSCs possesses a similar V_{OC}, but with significantly difference in J_{SC}. In these PSCs, the only difference is in the anode buffer layer. Therefore, it is reasonable to conclude that both Fe_3O_4 MNP and an external magnetostatic field have significant influences on J_{SC}.

To investigate enhanced J_{SC} from PSCs-(PEDOT:PSS):-Fe_3O_4 and PSCs-[(PEDOT:PSS):Fe_3O_4] W/H, we carried out X-ray photoelectron spectroscopy (XPS) to characterize the surface properties of PEDOT:PSS, (PEDOT:PSS):Fe_3O_4 and [(PEDOT:PSS):Fe_3O_4] W/H thin films. As shown in Figure 8a, the major components of the surface of all the three-type-films are the same. The partial enlarged Figure 8b shows that all these three thin films exhibit no typical peaks of Fe_3O_4 (Fe $2p_{1/2}$ and $2p_{3/2}$ peaked at 723.6 and 710.4 eV, respectively). These results indicate the Fe_3O_4 MNP are frozen inside the PEDOT:PSS thin film. Therefore, the possibility that the migration of Fe_3O_4 MNP into BHJ composite layer to enhance J_{SC} can be ruled out.

In PSCs, separated charge carriers have to be transported through the buffer layer to the respective electrodes. Thus, the anode buffer layer with high electrical conductivity is favorable to offer direct pathways for separated holes to be transported to the ITO anode. As described above, the electrical conductivity of the (PEDOT:PSS):Fe_3O_4 thin film is higher than that of PEDOT:PSS. Therefore, J_{SC} observed from PSCs-(PEDOT:PSS):Fe_3O_4 is higher than that of PSCs-(PEDOT:PSS). For PSCs-[(PEDOT:PSS):Fe_3O_4] W/H, in addition to the high electrical conductivity of (PEDOT:PSS):Fe_3O_4, the external magnetostatic filed probably also plays an important role in enhancing J_{SC}. In the presence of an external magnetostatic field, Fe_3O_4 MNP exhibits superparamagnetism at room temperature.[18] The randomly distributed Fe_3O_4 MNP within the PEDOT:PSS thin film could be self-assembled by the dipole−dipole interaction among Fe_3O_4 MNP.[28−30] This self-assembled Fe_3O_4 MNP certainly will enhance the electrical conductivity of (PEDOT:PSS):Fe_3O_4 thin film. Moreover, it has been reported that weak magnetic field can increase the dissociation ratio of triplet excitons, yielding a positive magnetoconductance and increasing the current through PSCs because of the long lifetime of the triplet excitons compared to that of the singlet excitons in conjugated polymers.[31,32] All these effects arouse from the addition of Fe_3O_4 MNP into PEDOT:PSS, followed with an external magnetostatic filed alignment, result in ∼38.5% enhancement in J_{SC}.

In order to further verify the electrical conductivities of these three thin films, the internal series resistances (R_S) of these three PSCs were investigated by impedance spectroscopy (IS). The IS analysis enables us to monitor the detailed electrical properties of the interface that cannot be determined by direct current measurements. The R_S is composed of the sheet resistance (R_{Sh}) of the electrodes, the charge-transfer resistance (R_{CT}) at the interfaces between the ITO anode and buffer layer, and the anode buffer and BHJ active layer, inside of BHJ active layer.[33] For these three PSCs, the only difference is the R_{CT} at the interfaces between the ITO anode and buffer layer, between the anode buffer and BHJ active layer. Figure 9 shows the

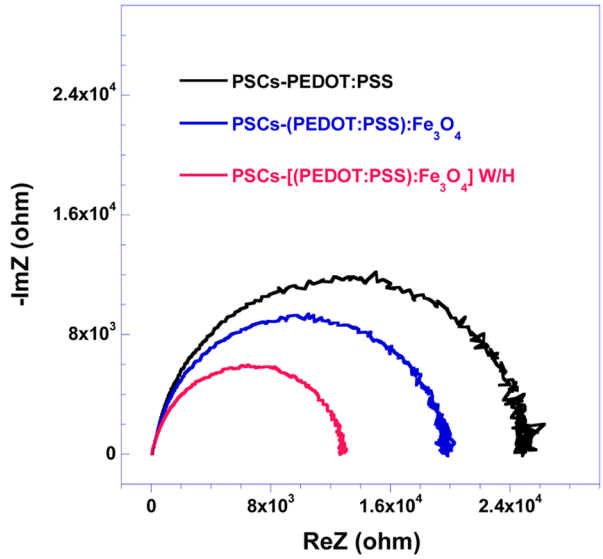

Figure 9. Nyquist plots of PSCs measured under 100 mW cm^{-2} AM 1.5 G illumination.

Nyquist plots of PSCs measured under the light intensity of 100 mW cm^{-2} and at the applied voltage of 0.78 V. From the plots, R_{CT} of 13, 19, and 25 kΩ are observed from PSCs-[(PEDOT:PSS):Fe_3O_4] W/H, PSCs-(PEDOT:PSS):Fe_3O_4 and PSCs-PEDOT:PSS, respectively. These results indicated that electrical conductivity of [(PEDOT:PSS):Fe_3O_4] W/H thin film is indeed higher than that of (PEDOT:PSS):Fe_3O_4 thin film, which is higher than that of PEDOT:PSS thin film. Therefore, the magnetostatic field can induce rearrangement of film morphology of (PEDOT:PSS):Fe_3O_4 at nanoscale, resulting in not only enhanced charge transport inside the buffer layer, but also reduced interfacial series resistance.[34] As a result, enlarged J_{SC} is observed from PSCs-[(PEDOT:PSS):-Fe_3O_4] W/H.

The stabilities of all three PSCs were also studied. The stability was tested from the devices that are encapsulated under an inert atmosphere with a glass lid, and epoxy glue Figure 10 compares the shelf-stabilities of PSCs-PEDOT:PSS, PSCs-(PEDOT:PSS):Fe_3O_4 and PSCs-[(PEDOT:PSS):Fe_3O_4] W/H, respectively. Because PSCs have a conventional architecture of ITO/buffer layer/BHJ active layer/Ca/Al, the degradation is caused by hygroscopic and acidic erosion caused by PEDOT:PSS, and oxidation of top metals (Ca coated by Al).[35−37] To compare the stability influenced by the anode buffer layer, we encapsulated all PSCs to minimize contribution

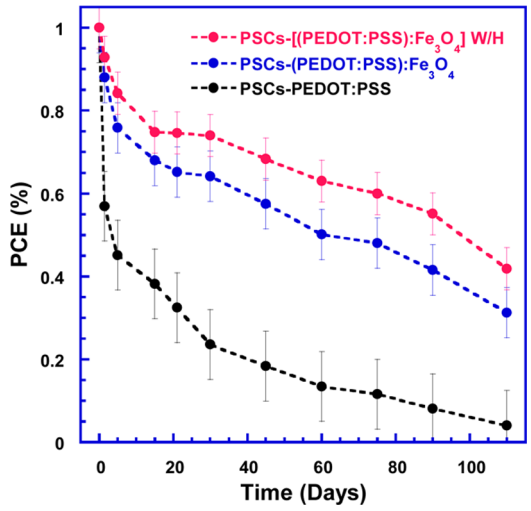

Figure 10. Stabilities of PSCs-PEDOT:PSS, PSCs-(PEDOT:PSS):-Fe_3O_4, and PSCs-[(PEDOT:PSS):Fe_3O_4] W/H, respectively.

of oxidation of the top metal electrode. PCE of PSCs-[(PEDOT:PSS):Fe_3O_4] W/H remains approximately 55% of the original value after 90 days; the PCE of PSCs-(PEDOT:PSS):Fe_3O_4 remains approximately 55% of the original value after 85 days, while the PCE of PSCs-PEDOT:PSS degrades evidently after only 12 h and remains 50% of the original value after 5 days. These results demonstrate that the stability of PSCs by using the thin films of (PEDOT:PSS):Fe_3O_4 and [(PEDOT:PSS):Fe_3O_4] W/H, respectively, are significantly improved as compared with those by using PEDOT:PSS thin film as an anode buffer layer.

CONCLUSIONS

In conclusion, we have successfully demonstrated that enhanced efficiency and improved stability of PSCs can be realized by using a thin film fabricated from the solution of PEDOT:PSS-doped Fe_3O_4 magnetic nanoparticles, and the above thin film aligned by an external magnetostatic field as an anode buffer layer, respectively; 38.5% enhanced efficiency and twice improved stability resulted from a combination of reduced acidity of PEDOT:PSS and enhanced electrical conductivity, which originated from generated counterions and the paramagnetism of Fe_3O_4 magnetic nanoparticles by an external magnetostatic field. Our results certainly inspire a new approach toward the low-cost manufacturing of polymer (organic) solar cells with both high efficiency and good stability.

AUTHOR INFORMATION

Corresponding Author

*E-mail: xgong@uakron.edu.

Author Contributions

†Authors K.W. and C.Y. contributed equally to this work

Notes

The authors declare no competing financial interest.

ACKNOWLEDGMENTS

The authors at the University of Akron thank NSF (1351785) for financial support. The authors acknowledge Dr. Bojie Wang and Dr. Xuehui Dong for assistance with TEM measurements.

REFERENCES

(1) Gunes, S.; Neugebauer, H.; Sariciftci, N. S. Conjugated Polymer-based Organic Solar Cells. *Chem. Rev.* **2007**, *107*, 1324−1338.
(2) Yang, T.; Wang, M.; Duan, C.; Hu, X.; Huang, L.; Peng, J.; Huang, F.; Gong, X. Inverted Polymer Solar Cells with 8.4% Efficiency by Conjugated Polyelectrolyte. *Energy. Environ. Sci.* **2012**, *5*, 8208−8214.
(3) Dennler, G.; Scharber, M. C.; Brabec, C. J. Polymer-Fullerene Bulk-Heterojunction Solar Cells. *Adv. Mater.* **2009**, *21*, 1323−1338.
(4) Peumans, P.; Forrest, S. R. Very-High-Efficiency Double-Heterostructure Copper Phthalocyanine/C60 Photovoltaic Cells. *Appl. Phys. Lett.* **2001**, *79*, 126−128.
(5) Sun, Y.; Seo, J. H.; Takacs, C. J.; Seifter, J.; Heeger, A. J. Inverted Polymer Solar Cells Integrated with A Low-Temperature-Annealed Sol-Gel-Derived ZnO Film as an Electron Transport Layer. *Adv. Mater.* **2011**, *23*, 1679−1683.
(6) Yang, T.; Wang, M.; Cao, Y.; Huang, F.; Huang, L.; Peng, J.; Gong, X.; Cheng, S. Z. D.; Cao, Y. Polymer Solar Cells with a Low-Temperature-Annealed Sol−Gel-Derived MoOx Film as a Hole Extraction Layer. *Adv. Energy Mater.* **2012**, *2*, 523−527.
(7) Girtan, M.; Rusu, M. Role of ITO and PEDOT:PSS in Stability/Degradation of Polymer:Fullerene Bulk Heterojunctions Solar Cells. *Sol. Energy Mater. Sol. Cells* **2010**, *94*, 446−450.
(8) Argun, A. A.; Cirpan, A.; Reynolds, J. R. The First Truly All-Polymer Electrochromic Devices. *Adv. Mater.* **2003**, *15*, 1338−1341.
(9) Ouyang, J.; Xu, Q.; Chu, C. W.; Yang, Y.; Li, G.; Shinar, J. On the Mechanism of Conductivity Enhancement in Poly(3,4-ethylenedioxythiophene):Poly(styrene sulfonate) Film Through Solvent Treatment. *Polymer* **2004**, *45*, 8443−8450.
(10) Tseng, Y. C.; Mane, A. U.; Elam, J. W.; Darling, S. B. Ultrathin Molybdenum Oxide Anode Buffer Layer for Organic Photovoltaic Cells Formed Using Atomic Layer Deposition. *Sol. Energy Mater. Sol. Cells* **2011**, *99*, 235−239.
(11) Shrotriya, V.; Li, G.; Yao, Y.; Chu, C. W.; Yang, Y. Transition Metal Oxides as the Buffer Layer for Polymer Photovoltaic Cells. *Appl. Phys. Lett.* **2006**, *88*, 073508−3.
(12) Gong, C.; Yang, H. B.; Song, Q. L.; Li, C. M. Nanostructure Effect of V_2O_5 Buffer Layer on Performance of Polymer-Fullerene Devices. *Org. Electron.* **2012**, *13*, 7−12.
(13) Kim, D. Y.; Subbiah, J.; Sarasqueta, G.; So, F.; Ding, H.; Irfan; Gao, Y. The Effect of Molybdenum Oxide Interlayer on Organic Photovoltaic Cells. *Appl. Phys. Lett.* **2009**, *95*, 093304.
(14) Stubhan, T.; Ameri, T.; Salinas, M.; Krantz, J.; Machui, F.; Halik, M.; Brabec, C. J. High Shunt Resistance in Polymer Solar Cells Comprising a MoO_3 Hole Extraction Layer Processed From Nanoparticle Suspension. *Appl. Phys. Lett.* **2011**, *98*, 253308.
(15) Po, R.; Carbonera, C.; Bernardi, A.; Camaioni, N. The Role of Buffer Layers in Polymer Solar Cells. *Energy Environ. Sci.* **2010**, *4*, 285−310.
(16) Fang, G.; Wu, S.; Xie, Z.; Geng, Y.; Wang, L. Enhanced Performance for Polymer Solar Cells by Using Surfactant-Modified PEDOT:PSS as the Anode Buffer Layer. *Macromol. Chem. Phys.* **2011**, *212*, 1846−1851.
(17) Han, Y. K.; Chang, M. Y.; Huang, W. Y.; Pan, H. Y.; Ho, K. S.; Hsieh, T. H.; Pan, S. Y. Improved Performance of Polymer Solar Cells Featuring One-Dimensional PEDOT Nanorods in a Modified Buffer Layer. *J. Electrochem. Soc.* **2011**, *158*, K88−K93.
(18) Frey, N. A.; Peng, S.; Cheng, K.; Sun, S. Magnetic Nanoparticles: Synthesis, Functionalization, and Applications in Bioimaging and Magnetic Energy Storage. *Chem. Soc. Rev.* **2009**, *38*, 2532−2542.
(19) Jong, S. J.; Kim, C. S.; Kim, J. B.; Ryu, S. Y.; Noh, J. H.; Baik, H. K.; Kim, Y. S.; Lee, S.-J. Increase in Indium Diffusion by Tetrafluoromethane Plasma Treatment and its Effects on the Device Performance of Polymer Light-Emitting Diodes. *J. Appl. Phys.* **2008**, *103*, 114502.
(20) De Jong, M. P.; Van Ijzendoorn, L. J.; De Voigt, M. J. A. Stability of the Interface Between Indium-Tin-Oxide and Poly(3,4-

ethylenedioxythiophene)/Poly(styrenesulfonate) in polymer Light-Emitting Diodes. *Appl. Phys. Lett.* **2000**, *77*, 2255−2257.
(21) Danchick, R. S.; Boltz, D. F. Indirect Spectrophotometric and Atomic Absorption Spectrometric Methods for Determination of Thiocyanate. *Anal. Chem.* **1968**, *40*, 2215−2216.
(22) Xia, Y.; Ouyang, J. Highly Salt-Induced Charge Screening and Significant Conductivity Enhancement of Conducting Poly(3,4-ethylenedioxythiophene):Poly(styrenesulfonate). *Macromolecules* **2009**, *42*, 4141−4147.
(23) Xia, Y.; Zhang, H.; Ouyang, J. Highly Conductive PEDOT:PSS Films Prepared Through a Treatment with Zwitterions and Their Application in Polymer Photovoltaic Cells. *J. Mater. Chem.* **2010**, *20*, 9740−9747.
(24) Xia, Y.; Sun; Ouyang, J. Solution-Processed Metallic Conducting Polymer Films as Transparent Electrode of Optoelectronic Devices. *Adv. Mater.* **2012**, *24*, 2436−2440.
(25) Lu, H. S.; Song, H. J.; Shi, H.; Jiang, Q. L.; Zhang, L.; Liu, C. C.; Xu, J. K. Preparation of Poly (3,4-ethylenedioxythiophene)-Poly-(styrenesulfonate)/Fe_3O_4 Nanocomposite Film and its Thermoelectric Performance. *J. Compos. Mater.* **2013**, *0*, 1−9.
(26) Li, C. Z.; Minne, S.; Pittenger, B.; Mednick, A.; Guide, M.; Nguyen, T.-Q. *Simultaneous Electrical and Mechanical Property Mapping at the Nanoscale with PeakForce TUNA*; Bruker Nano Surfaces Division, Santa Barbara, CA, 2011.
(27) Huo, L.; Zhang, S.; Guo, X.; Xu, F.; Li, Y.; Hou, J. Replacing Alkoxy Groups with Alkylthienyl Groups: A Feasible Approach To Improve the Properties of Photovoltaic Polymers. *Angew. Chem., Int. Ed.* **2011**, *50*, 9697−9702.
(28) Mørup, S.; Hansen, M. F.; Frandsen, C. Magnetic Interactions between Nanoparticles. *Beilstein J. Nanotechnol.* **2010**, *1*, 182−190.
(29) Sheparovych, R.; Sahoo, Y.; Motornov, M.; Wang, S.; Luo, H.; Prasad, P. N.; Sokolov, I.; Minko, S. Polyelectrolyte Stabilized Nanowires from Fe_3O_4 Nanoparticles via Magnetic Field Induced Self-Assembly. *Chem. Mater.* **2006**, *18*, 591−593.
(30) Sahoo, Y.; Cheon, M.; Wang, S.; Luo, H.; Furlani, E. P.; Prasad, P. N. Field-Directed Self-Assembly of Magnetic Nanoparticles. *J. Phys. Chem. B* **2004**, *108*, 3380−3383.
(31) Wu, Y.; Hu, B. Metal Electrode Effects on Spin-Orbital Coupling and Magnetoresistance in Organic Semiconductor Devices. *Appl. Phys. Lett.* **2006**, *89*, 203510.
(32) Xu, Z.; Hu, B. Photovoltaic Processes of Singlet and Triplet Excited States in Organic Solar Cells. *Adv. Funct. Mater.* **2008**, *18*, 2611−2617.
(33) Kim, J.-S.; Chung, W.-S.; Kim, K.; Kim, D. Y.; Paeng, K.-J.; Jo, S. M.; Jang, S.-Y. Performance Optimization of Polymer Solar Cells Using Electrostatically Sprayed Photoactive Layers. *Adv. Funct. Mater.* **2010**, *20*, 3538−3546.
(34) Alemu, D.; Wei, H.-Y.; Ho, K.-C.; Chu, C.-W. Highly Conductive PEDOT:PSS Electrode by Simple Film Treatment with Methanol for ITO-Free Polymer Solar Cells. *Energy Environ. Sci.* **2012**, *5*, 9662−9671.
(35) Hutter, O. S.; Stec, H. M.; Hatton, R. A. An Indium-Free Low Work Function Window Electrode for Organic Photovoltaics Which Improves with In-Situ Oxidation. *Adv. Mater.* **2013**, *25*, 284−288.
(36) Wang, M.; Xie, F.; Du, J.; Tang, Q.; Zheng, S.; Miao, Q.; Chen, J.; Zhao, N.; Xu, J. B. Degradation Mechanism of Organic Solar Cells with Aluminum Cathode. *Sol. Energy Mater. Sol. Cells* **2011**, *95*, 3303−3310.
(37) Voroshazi, E.; Verreet, B.; Buri, A.; Müller, R.; Di Nuzzo, D.; Heremans, P. Influence of Cathode Oxidation via the Hole Extraction Layer in Polymer:Fullerene Solar Cells. *Org. Electron.* **2011**, *12*, 736−744.